metals

MDPI

Article

An Experimental Investigation about the Dimensional Accuracy and the Porosity of Copper-Filled PLA Fused Filament Fabrication Parts

Irene Buj-Corral [1,*] and Maurici Sivatte-Adroer [2]

[1] Department of Mechanical Engineering, Barcelona School of Industrial Engineering (ETSEIB), Universitat Politècnica de Catalunya, Av. Diagonal, 647, 08028 Barcelona, Spain
[2] Department of Mechanical Engineering, Polytechnic School of Engineering of Vilanova i la Geltrú (EPSEVG), Universitat Politècnica de Catalunya, Av. Víctor Balaguer, 1, 08880 Geltrú, Spain; maurici.sivatte@upc.edu
* Correspondence: irene.buj@upc.edu; Tel.: +34-934054015

Abstract: In recent years, metal-filled plastic filaments have begun to be used in fused filament fabrication (FFF) technology. However, the characterization of the parts obtained is still under development. In this work, the results on dimensional accuracy and porosity of copper-filled 3D-printed parts are presented. Cuboid parts were 3D-printed in the vertical position. The three dimensions of each part were measured, and the relative error was calculated for each one of them. Dimensional accuracy in terms of width and depth depends mainly on the layer height and printing temperature, while accuracy in height is mainly influenced by print speed and the interaction of layer height with print speed. Porosity is related to layer height, printing temperature and print speed. According to multiobjective optimization, to minimize dimensional error and obtain a porosity target value of 20%, it is recommended to select a low layer height of 0.1 mm, a high print speed of 40 mm/s, a low extrusion multiplier of 0.94 and a low temperature of 200 °C. The results of the present work will help to select appropriate 3D printing parameters when using metal-filled filaments in FFF processes.

Keywords: copper-filled filament; PLA; FFF; FDM; dimensional accuracy; porosity

Citation: Buj-Corral, I.; Sivatte-Adroer, M. An Experimental Investigation about the Dimensional Accuracy and the Porosity of Copper-Filled PLA Fused Filament Fabrication Parts. *Metals* **2023**, *13*, 1608. https://doi.org/10.3390/met13091608

Academic Editors: Matteo Benedetti and Emin Bayraktar

Received: 2 August 2023
Revised: 4 September 2023
Accepted: 12 September 2023
Published: 18 September 2023

1. Introduction

In recent years, metal-filled polymeric filaments have bloomed in the market of fused deposition modeling (FDM) or fused filament fabrication (FFF) supplies. Different metals are commonly used for this purpose, such as stainless steel [1], titanium, bronze and copper, in a process that is known as metal FDM [2].

Copper (Cu) has been used to manufacture parts at least from 5000 BC [3]. Due to its high electrical and thermal conductivity, its good workability, and its high corrosion resistance, it is widely employed in industrial applications like the manufacture of electric and electronic devices, since it improves the electrical and thermal conductivity of the components [3–5]. It is used in steel alloys to improve the corrosion resistance and mechanical properties of the alloy [6]. Copper is employed in the pharmaceutical industry, for example with the addition of copper traces to creams [3]. It is also known to have antibacterial properties and, for this reason, it is employed in hospital equipment and utensils [7]. In addition to metallic copper, some copper–polymer composites have antibacterial properties, specifically polyamide 12 with cuprous oxide (Cu_2O) [8]. Regarding other metals, steel-filled PLA favor cell growth, while bronze and silver have the opposite behavior and can be used as scaffolds in tissue engineering [9,10]. Another application of metal-filled polymers is their use in heat sinks [11]. They allow for the dissipation of heat when either biocompatibility (in implants, for example) or electrical insulation (in electronic devices, for instance) is required. Another advantage of metal-filled polymers is that the heat expansion coefficient can be reduced, thus reducing distortion during the 3D-printing process, as in ABS matrices filled with iron and copper particles [12,13].

As for the additive manufacturing of metal-filled plastic materials, for example, resins with copper nano-inclusions were used with the VAT-polymerization (VPP) technique in a work by Vidakis et al. [14]. They found that adding 0.5 wt. % of Cu improved the mechanical properties of the material, by 11% in tensile strength and 10% in flexural strength. Regarding the FFF technology, the use of metal-filled plastic filaments is still under development [15]. One of the first examples on 3D printing of stainless-steel parts with polymeric matrix corresponds to Wu et al. in 2002 [16]. As for Cu, Singh et al. [17] used both Nylon and acrylonitrile-butadiene-styrene (ABS)-copper-filled filaments. They found that the addition of small copper particles (200 and 400 mesh) increased the flow of the material, as well as its tensile strength, making it possible to obtain copper-filled plastic filaments. Nevertheless, other authors found a decrease in the mechanical properties of the composite material if larger quantities of metal were added [18]. For example, in PLA matrices, Fafenrot et al. reported lower tensile strength values when bronze was used [19]. Kotassamy et al. found that when increasing the Cu content in PLA matrix filaments from 25 wt. % to 80 wt. %, ultimate tensile strength was reduced from 13.55 MPa to 4.16 MPa for the rectilinear infill pattern [20]. However, the filament containing 80 wt. % Cu showed higher stiffness than the filament containing 25 wt. %. Balamurugan et al. [21] used Cu-filled PLA filament with Cu content up to 20 wt. %. They observed that high printing temperature of 230 °C, high bed temperature of 70 °C, and medium layer thickness of 0.14 mm provided the highest compressive strength of 32.85 MPa. However, in the work by Prajapati et al., higher compressive strength values of up to 67 MPa were reported [22]. In ABS material, Sa'ude et al. [23] added different quantities of Cu, of up to 26% in volume. They observed that the dynamic mechanical properties of the filament were affected by the quantity of copper. The same authors found that higher temperature and higher feed rate were required to print ABS when it was filled with copper [24]. In addition, Cu-filled ABS filaments with Cu content up to 40 vol. % showed higher stiffness than ABS filaments [13]. Hwang et al. [12] reported a decrease in the tensile strength of Cu-filled ABS parts when copper content was increased from 10% (42 MPa) to 30% (26.5 MPa). These results suggest that, as a general trend, the presence of metallic Cu within the filament reduces the mechanical strength of the FFF 3D-printed parts when compared to 100% plastic filaments, provided that similar printing conditions are employed. However, the use of Cu as an oxide could enhance the mechanical properties of the 3D-printed materials. For example, when adding Cu as cuprous oxide and as well as cellulose nanofibers to PLA, Petousis et al. reported an increase in the mechanical properties of the 3D-printed samples compared to those containing only PLA [25]. Specifically, when 0.5 wt. % Cu_2O and 1.0 wt. % cellulose nanofibers were used, tensile strength increased by 51.1% and flexural strength increased by 23.2%.

Dimensional accuracy is usually addressed in manufacturing processes to test if the parts will comply with dimensional requirements [26]. For additively manufactured parts, for example, in selective laser sintering (SLS), Islam et al. [27] found that the dimensions in the xy plane were undersized, while the dimensions in the z direction were oversized. In FFF processes with polylactic acid (PLA), Vidakis et al. [28] reported that bed temperature and nozzle temperature had the greatest effect on dimensional accuracy of the parts, while layer thickness and infill density were the most influential parameters on porosity. In a similar work with ABS, the same authors observed that dimensional accuracy mainly depended on bed temperature and print speed, and porosity was influenced by infill density and raster angle [29]. When 3D-printing hemispherical cups in PLA, Luis-Pérez et al. [30] found dimensional error values of up to 0.361 mm in a diameter of 50 mm (0.7% relative error). As for ABS parts, Rahman et al. [31] recommended low bed temperature, low printing temperature, high print speed, medium infill rate, low layer thickness, and low shell thickness to obtain low dimensional error. In polycaprolactone (PCL) parts, Ceretti et al. [32] found that the nominal size of pores was directly related to the filament diameter once extruded. On the other hand, Nancharaiah et al. [33] reported that low layer thickness and bead width favored the dimensional accuracy of the parts. Pennington

et al. [34] observed that part size, location of the part on the printing bed and the envelope temperature had a great influence on dimensional accuracy. Caminero et al. [35] reported high dimensional accuracy in PLA and PLA–graphene 3D-printed parts in the z direction, when both the flat and on-edge orientations were selected.

Porosity and pore size are important properties in tissue engineering [36,37]. In FFF 3D-printed parts, for instance, Too et al. [38] obtained porous structures with controlled porosity using the cross-hatch pattern in ABS material, with porosity values ranging from 20% to 70% and average pore diameter between 0.05 and 0.35. Buj-Corral et al. [39] modeled porosity and pore size in 3D printed PLA parts with the grid structure, with porosity values of 20%, 40%, 60%, and 80%, and pore size between 0 and 2 mm. Ali et al. [40] 3D-printed spherical cell porous structures, with porosity values between 83% and 89%. They found that using hexagonal packing, open porosity and a loading direction parallel to the manufacturing direction provided the best mechanical properties among the different structures that were tested. Porosity can be measured by different methods; for example, the Archimedes method [41], computerized tomography (CT) [28], or the measurement and weight of the samples [42].

However, dimensional accuracy and porosity of metal-filled plastic 3D-printed parts have been scarcely studied in the literature. In the present work, copper-filled FFF 3D-printed parts are studied and analyzed. For this purpose, 3D-printing experimental tests were performed, in which four different parameters were varied: layer height, print speed, extrusion multiplier, and printing temperature. Cuboid samples were obtained, and their three dimensions were measured with a micrometer. The samples were also weighed with a precision scale. Three relative error values were calculated, corresponding to X, Y, and Z dimensions, respectively. In addition, the total relative error value was determined. Porosity was calculated from the weight and dimensions of the specimens. Multi-objective optimization was carried out to simultaneously minimize dimensional error and obtain a target porosity value of 20%.

2. Materials and Methods

2.1. 3D Printing of the Specimens

A Sigma R19 3D-printer from BCN3D Technologies (Gavà, Spain) was employed. A 2.85 mm diameter copper-filled filament was used from Colorfabb (Belfeld, The Netherlands), with polylactic acid (PLA) as the matrix material. The density of the filament is 4.0 g/cm^3, corresponding to approximately 35 wt. % Cu in weight. Other specifications of the filament are: humidity absorption 0.3%, tensile strength 25 MPa and flexural strength 40 MPa [43].

Cuboid specimens of theoretical dimensions 10 × 10 × 20 mm were printed with no shell (Figure 1). The infill pattern was rectilinear at −45° and 45°, respectively. This corresponds to alternated layers: one layer with parallel filaments with raster angle 45° and the following one with parallel filaments with raster angle −45° (resulting in 90° between them). Infill ratio value was 80%, corresponding to a porosity value of 20%. Nozzle diameter was 0.4 mm. The specimens were printed one by one, all of them in the middle of the building platform.

A factorial design allows for a set of experiments to be defined with different factors and different levels. This type of design helps to study the influence of the factors, as well as their interactions, on the responses. A full factorial 2^4 design was used in this work, with 4 variables and 2 levels. According to the previous experience with PLA filament, the selected variables were layer height, print speed, extrusion multiplier and printing temperature. The upper and lower limits for the variables are presented in Table 1. A central point was added to the design (experiment 17 in Table 2, with 3 replicates), in order to assess if the models show curvature.

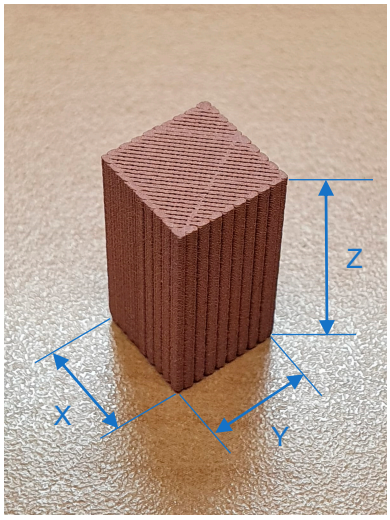

Figure 1. Prismatic sample obtained in copper-filled material.

Table 1. Variables, lower and upper limits.

Variable	Acronym	Lower Limit	Upper Limit
Layer height (mm)	LH	0.1	0.3
Print speed (mm/s)	PS	30	40
Extrusion multiplier	EM	0.94	1
Printing temperature (°C)	PT	200	220

Table 2. Dimensional errors Edx, Edy, Edz, Edt, Mass and Porosity P.

Experiment	LH (mm)	PS (mm/s)	EM	PT (°C)	Edx (%)	Edy (%)	Edz (%)	Edt (%)	Mass (g)	P (%)
1	0.1	20	0.94	200	0.00	0.90	1.25	0.72	6.14	16.99
2	0.3	20	0.94	200	2.20	3.30	3.25	2.92	5.90	26.20
3	0.1	40	0.94	200	0.20	1.30	1.25	0.92	6.13	19.07
4	0.3	40	0.94	200	2.80	3.60	1.05	2.48	5.20	35.60
5	0.1	20	1	200	0.20	1.10	1.50	0.93	6.44	15.25
6	0.3	20	1	200	2.50	3.50	1.80	2.60	5.69	29.24
7	0.1	40	1	200	0.50	1.60	1.15	1.08	6.23	18.85
8	0.3	40	1	200	3.30	4.30	1.00	2.87	5.48	33.68
9	0.1	20	0.94	220	0.10	1.20	1.45	0.92	6.62	10.61
10	0.3	20	0.94	220	3.00	4.30	2.15	3.15	6.37	21.88
11	0.1	40	0.94	220	0.80	1.90	1.45	1.38	6.37	18.32
12	0.3	40	0.94	220	4.20	5.50	1.05	3.58	6.23	24.56
13	0.1	20	1	220	0.20	1.40	1.45	1.02	6.99	7.46
14	0.3	20	1	220	3.80	5.30	1.95	3.68	6.72	17.06
15	0.1	40	1	220	0.90	1.50	1.45	1.28	6.93	8.34
16	0.3	40	1	220	5.20	5.80	1.10	4.03	6.78	18.96
17-1	0.2	30	0.97	210	1.70	3.10	1.70	2.17	6.28	20.60
17-2	0.2	30	0.97	210	1.70	3.3	1.75	2.25	6.21	22.28
17-3	0.2	30	0.97	210	1.70	3.2	1.75	2.22	6.23	24.13

The slicing program was Cura BCN3D. The samples were printed in the vertical position, in which the height of the cuboid corresponds to the Z direction of the machine. The three dimensions X, Y and Z of the specimens (Figure 1) were measured using a Mitutoyo micrometer. Each dimension was measured in the central part of the specimens. For example, dimension Z (total theoretical height of 20 mm) was measured 10 mm apart. Three measurements were taken for each specimen and direction, and the average value was calculated.

Five responses were considered. The calculation method for each response is presented in Section 2.2:

- Dimensional relative error along x axis: Edx, according to Equation (1).
- Dimensional relative error along y axis: Edy.
- Dimensional relative error along z axis: Edz.
- Average dimensional error Edt, according to Equation (2).
- Porosity P, according to Equation (3).

2.2. Measurement of the Samples

The dimensions of the samples were measured with a Mitutoyo micrometer with precision of 0.01 mm. Dimensional relative error along axis X was calculated according to Equation (1) (dimensional errors along axes Y and Z were calculated analogously).

$$\text{Edx } (\%) = \left| \frac{\text{Measured value dimension X} - \text{Theoretical Value dimension X}}{\text{Theoretical value dimension X}} \right| \cdot 100 \quad (1)$$

where:

Measured value dimension x is the measured value of dimension X with the micrometer, in mm.

Theoretical value is the nominal value of dimension X; in this case, 10 mm.

Total dimensional error was defined as the average value of the error along the x, y and Z directions, as per Equation (2).

$$\text{Edt } (\%) = \frac{\text{Edx} + \text{Edy} + \text{Edz}}{3} \quad (2)$$

The mass of the samples was determined with a Kern scale with precision 0.01 g.

Porosity P (%) was calculated according to Equation (3).

$$\text{P } (\%) = \frac{\rho_M - \rho_P}{\rho_M} \times 100 \quad (3)$$

where:

ρ_M = Density of the copper-filled material; in this case, 4 g/cm^3.

ρ_P = Density of the specimen in g/cm^3.

The density of each specimen was determined from their dimensions and their mass.

2.3. Mathematical Models and Multiobjective Optimization

Linear regression models were obtained for each of the selected responses. The Derringer—Suich desirability function [44] was used for the multiobjective optimization, with weight 1 (linear function), using the Minitab 20 software (Minitab LCC, State College, PA, USA).

Two different types of optimization were carried out:

- First, total dimensional error Edt was to be minimized, and a target value of 20% was defined for porosity P.
- Second, dimensional error along z axis Edz was to be minimized, and a target value of 20% was considered for porosity P.

In both studies, a first optimization run was performed, in which the same importance was given to both responses, and then a second optimization run was carried out, in which an importance value of 10 was given to one of the responses, while the importance of the other was kept at 1.

3. Results and Discussion

3.1. Dimensional Error and Porosity

The average values of the measured dimensions of the samples are presented in Figure 2 for X (Figure 2a), Y (Figure 2b) and Z (Figure 2c), respectively. The error bars show

± standard deviation of the measurements. The printing conditions of each experiment can be found in Table 2.

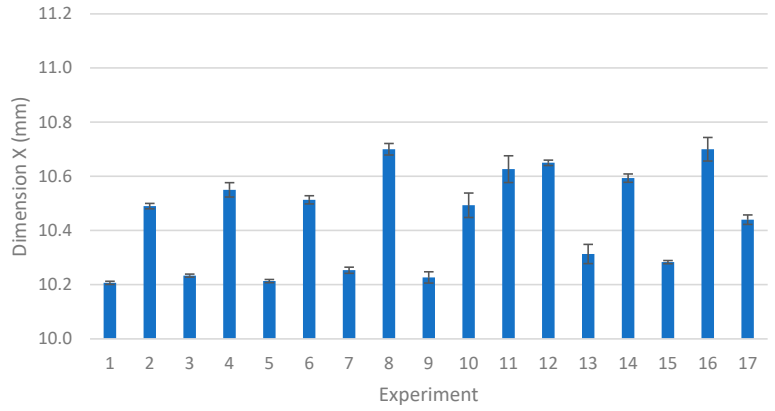

(**a**)

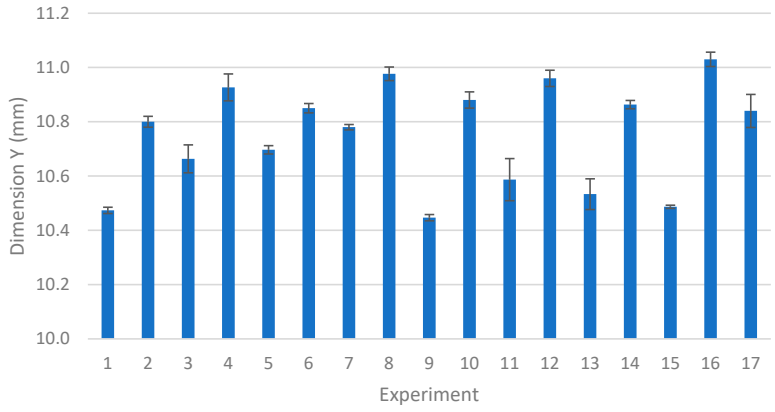

(**b**)

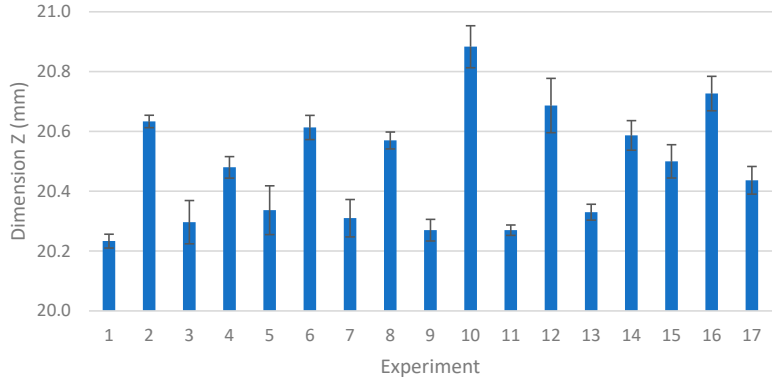

(**c**)

Figure 2. Dimensional measurements for the 19 experiments: (**a**) X (mm), (**b**) Y (mm), (**c**) Z (mm).

All the measured dimensions (X, Y and Z) are larger than the theoretical dimensions of 10 mm, 10 mm and 20 mm, respectively. As a general trend, experiments with high layer height provide larger dimensions than experiments with low layer height. This could be attributed to the calculations made by the slicing program or to the fact that the number of e-steps of the motors of the printing machine could not be adjusted to the single stepper motor that was used. This will be addressed in further research.

The results of the 17 experiments regarding dimensional error and porosity are shown in Table 2.

Dimensional error, mass and porosity depend on the printing conditions that were employed. For example, as a general trend, high layer height leads to high dimensional error and low porosity, below the target value of 20%. On the contrary, higher dimensional error and porosity above the target value are observed when high layer height is selected.

Although in principle the part should be isotropic on the XY plane, in this work different error values were observed in the X, Y and Z directions, respectively. For instance, Edy > Edx in all cases. This suggests a different behavior of the machine in the two different directions. In fact, axis X corresponds to the transversal direction, in which the displacement of each printing head is carried out along a transversal guide. On the contrary, axis Y corresponds to the longitudinal direction, in which the displacement of the whole transversal guide with the two printing heads is carried out with two lateral guides, which are placed one at each end of the transversal bar (Figure 3).

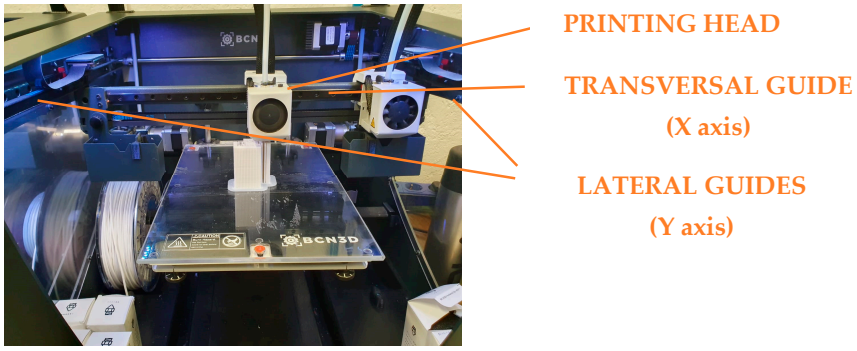

Figure 3. SigmaR19 3D printer from BCN3D Technologies.

Lowest Edx and Edy values correspond to experiments 1, 3 and 5, obtained with a low layer height of 0.1 mm and a low temperature of 200 °C. Highest Edx and Edy values were achieved in experiments 12, 14 and 16, which were printed with a high layer height of 0.3 and a high temperature of 220 °C. Thus, layer height and printing temperature have the greatest effect on Edx and Edy errors. The adhesion between layers worsens as layer height increases [45]. On the other hand, higher temperature will increase the fluidity of the material and dripping will be favoured [46,47].

As for Edz, as a general trend error values remain between 1.0 and 2.2%, except for experiment 2, with 3.25%. Highest Edz values correspond to experiments 2, 6, 10 and 14, obtained with a high layer height of 0.3 mm and a low print speed of 20 mm/s. This suggests that, in this case, higher speed should be used to avoid an excess of material on each layer, which would cause a too high part due to the stacking of thicker layers. On the contrary, lowest Edz values of around 1% were obtained in experiments 4, 8, 12 and 16, all of them with a high layer height of 0.3 mm and a high print speed of 40 mm/s. Thus, print speed is critical when addressing dimensional error in the Z direction. This difference with Edx/Edy can be attributed to the anisotropy of the part, which is obtained layer-by-layer, but also to the way the displacement in the z direction is produced, in which the building platform goes down as the part is printed.

Lowest total dimensional error Edt corresponds to experiment 1, obtained with a low layer height of 0.1 mm, a low speed of 20 mm/s, a low extrusion multiplier of 0.94 and a low temperature of 200 °C. Highest total dimensional error Edt was observed in experiment 16, with a high layer height of 0.3 mm, a high speed of 40 mm/s, a high extrusion multiplier of 1 and a high temperature of 220 °C. In general, the combination of high layer height and high temperature provides high total error values (experiments 16, 14, 12 and 10). On the other hand, the two different types of dimensional error (Edx/Edy and Edz) show the opposite behavior in some cases. For example, in experiments 1, 5, 9 and 13, low Edx/Edy but quite high Edz values are obtained. For these reasons, the multiobjective optimization is addressed in this work and presented in Section 3.3.

Lowest mass value of 5.20 g corresponds to experiment 4, with a high layer height, a high speed, a low extrusion multiplier and a low temperature. Highest mass value of 6.99 g was found in experiment 13, with a low layer height, a low speed, a high extrusion multiplier and a high temperature. As a general trend, lower mass values were obtained at low temperature than at high temperature. Temperature has been proven to affect melt flow rate in fused layer modelling (FLM) processes, for example [48]. When high printing temperature is considered (experiments 9–16), higher mass is observed for an extrusion multiplier value of 1 than for 0.94. This is due to the fact that higher extrusion multiplier value means wider beads and a higher flow of material [49,50]. However, when a low printing temperature is considered (experiments 1–8), both the extrusion multiplier and layer height have an important effect on mass. This could be attributed to a too low temperature, so that the material does not flow properly, and thus the amount of deposited material is lower than expected. This becomes more evident the higher the layer height. This effect was observed by Butt et al. for different materials, including PLA [47].

Lowest porosity values, below 8.5%, correspond to experiments 13 and 15, printed with a low layer height of 0.1 mm, a high extrusion multiplier of 1 and a high temperature of 220 °C. Highest porosity values, above 35%, correspond to experiments 4 and 8, with a high layer height of 0.3 mm, a high speed of 40 mm/s and a low temperature of 200 °C. Thus, layer height and temperature seem to have a great influence on porosity, as is true for Edx/Edy dimensional errors. This could be due to the fact that high layer height and low temperature (lower thermal expansion of the material) lead to bigger spaces between filaments.

3.2. Regression Models

From the results in Table 2, linear regression models were searched for Edx, Edy, Edz and P. Figure 4 shows the Pareto charts for Edx, Edy, Edz and Porosity, respectively.

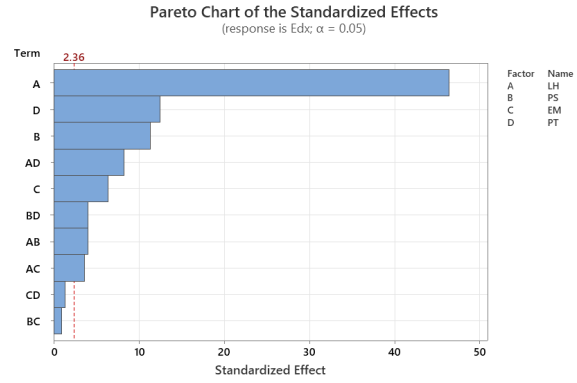

(**a**)

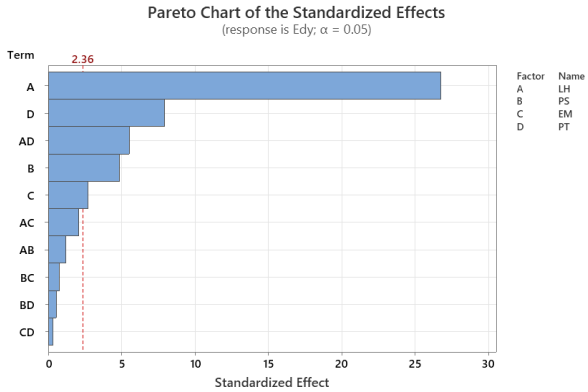

(**b**)

Figure 4. *Cont.*

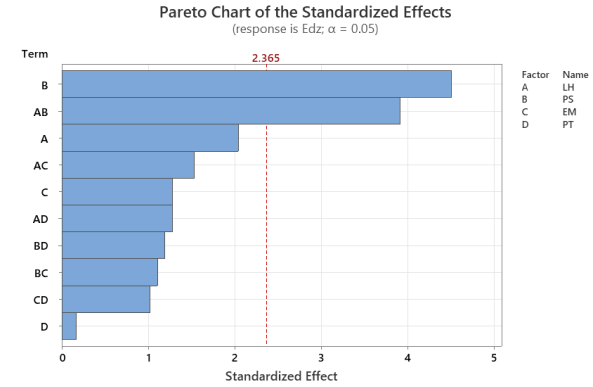

(**c**)

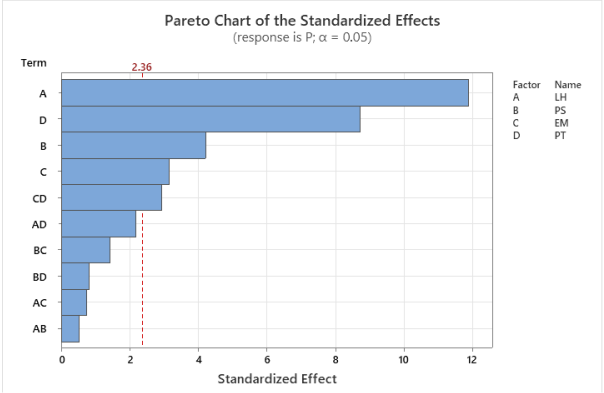

(**d**)

Figure 4. Pareto charts for: (**a**) Edx (%), (**b**) Edy (%), (**c**) Edz (%) and (**d**) porosity (%).

The main terms influencing Edx and Edy are layer height and printing temperature. Other authors have reported the great effect of layer height on dimensional accuracy in PLA 3D-printed parts [45,51]. Temperature worsens the dimensional accuracy for different materials, including PLA [46]. Edz is mainly influenced by print speed and the interaction of print speed with layer height.

As for porosity, the main terms of the model are layer height, printing temperature and print speed. Layer height is known to influence porosity in PLA 3D-printed parts [52–54], as well as porosity [55].

Figure 5 shows the main effects plot and the interaction plot for Edx.

The most influential factor on Edx is layer height, followed by printing temperature (Figure 5a). Reducing layer height, printing temperature, print speed and extrusion multiplier leads to lower dimensional error along the X direction, Edx (%). The most influential interaction is layer height·printing temperature (Figure 5b). If a low layer height is used, low Edx is achieved regardless of printing temperature. On the contrary, if a high layer height is selected, Edx depends on temperature. Using low layer height helps to deposit the material in a more uniform way, thus reducing the lateral displacement of the layers and leading to low dimensional error. When printing iron-filled PLA composites with 45 wt. % iron content, Darsin et al. [56] found that raster angle (which is not varied in the present work), layer height and printing temperature were most influential factors on dimensional accuracy.

Figure 6 corresponds to the main effects plot and the interaction plot for Edy.

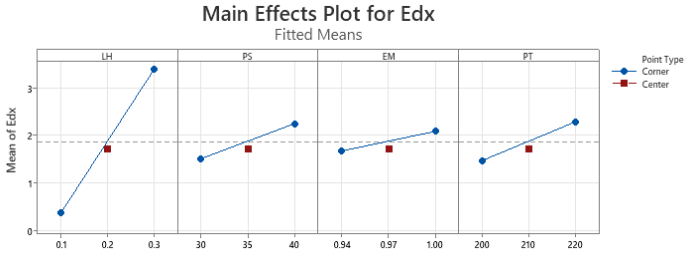

(**a**)

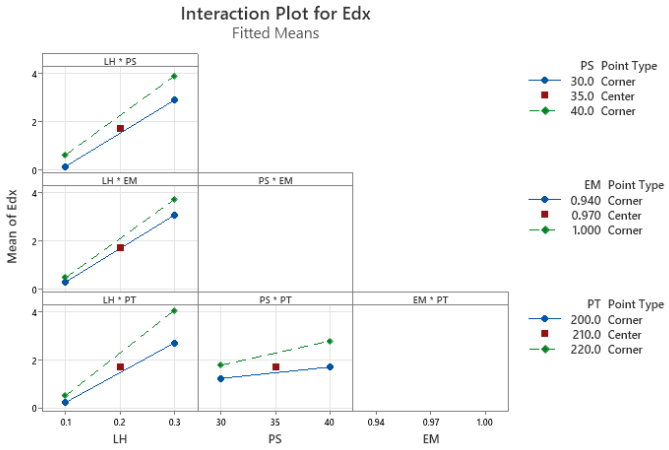

(**b**)

Figure 5. Plots for Edx: (**a**) main effects plot, (**b**) interaction plot. * stands for the multiplication symbol.

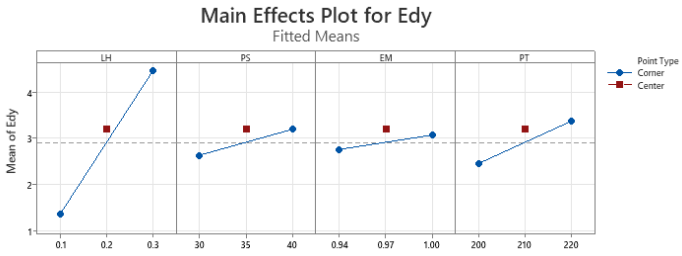

(**a**)

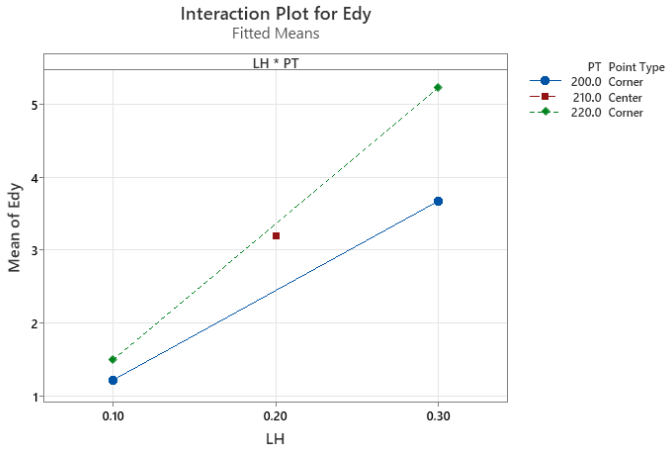

(**b**)

Figure 6. Plots for Edy: (**a**) main effects plot, (**b**) interaction plot. * stands for the multiplication symbol.

The results for Edy are similar to those for Edx, i.e., a low error is achieved if a low layer height of 0.1 mm, a low printing temperature of 200 °C, a low print speed of 30 mm/s and a low extrusion multiplier of 0.94 are selected. In this case, however, only the interaction between layer height and printing temperature is significant. A low dimensional error will be obtained if a low layer height is selected, regardless of the printing temperature used.

Figure 7 depicts the main effects plot and the interaction plot for Edz.

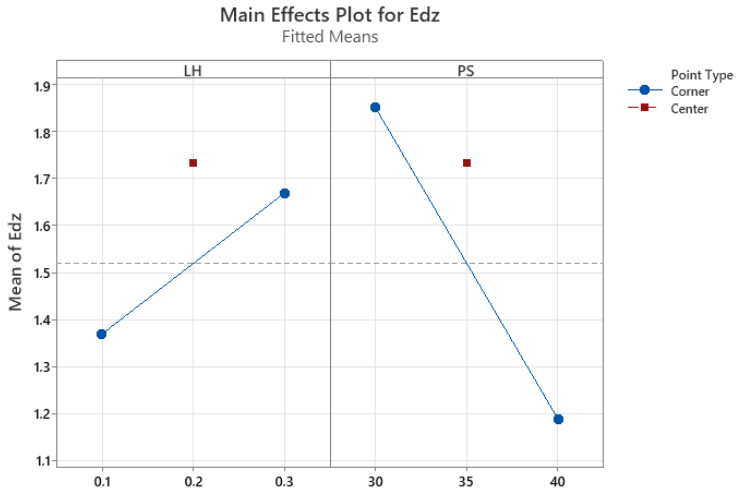

(**a**)

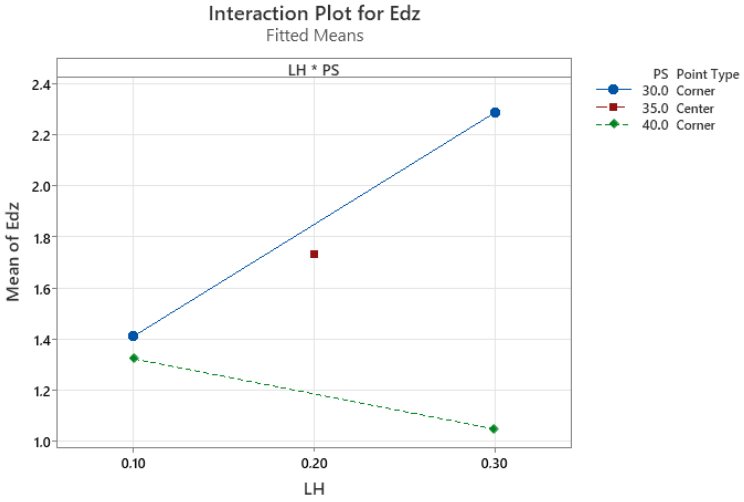

(**b**)

Figure 7. Plots for Edz: (**a**) main effects plot, (**b**) interaction plot. * stands for the multiplication symbol.

Dimensional error in the Z direction, Edz, depends mainly on printing speed and layer height: a high print speed of 40 mm/s and a low layer height of 0.1 mm will provide lower Edz values. Although a low layer height leads to quite low Edz values, unlike what happened for Edx and Edy, in this case, the combination of a high layer height of 0.3 mm and a high print speed of 40 mm/s leads to the lowest Edz values. If a low print speed is used, there might be an excess of material, with higher dimensional error in the Z axis, along which the consecutive layers are stacked (Figure 7a). This effect is clearer when a low speed is combined with a high layer height (experiments 2, 6, 10 and 14 in Table 2 and Figure 7b).

Figure 8 shows the main effects plot and the interaction plot for P.

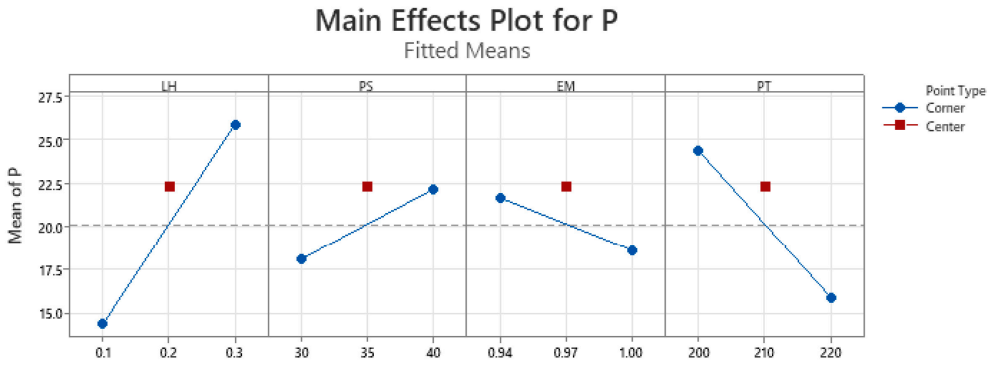

(**a**)

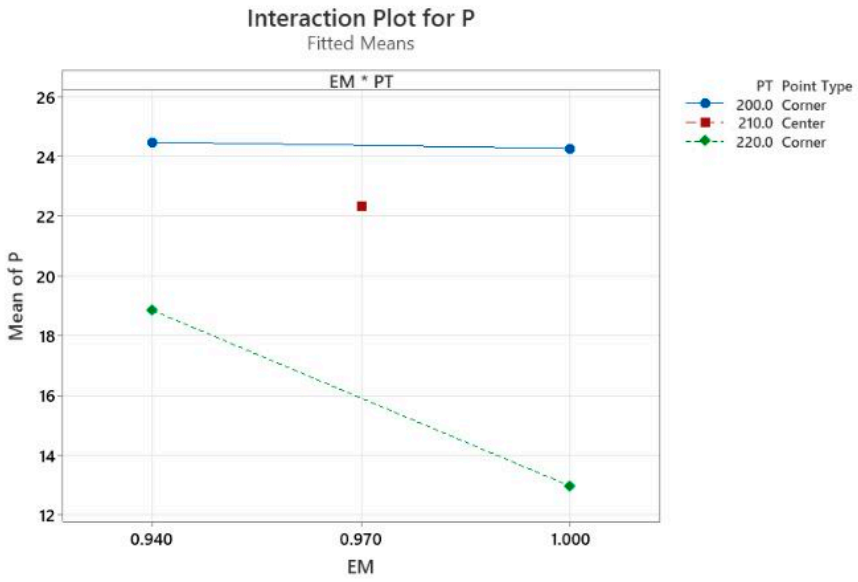

(**b**)

Figure 8. Plots for P: (**a**) main effects plot, (**b**) interaction plot.

The most influential term on porosity is layer height, followed by printing temperature (Figure 8a). A low layer height of 0.1 mm, a low print speed of 30 mm/s, a high printing temperature of 220 °C and a high extrusion multiplier of 1 will lead to low porosity. The use of a low layer height is known to reduce porosity, for example in ABS material [52]. For a certain extrusion multiplier value, which is related to a defined cross-sectional area of the filament, if layer height decreases the bead is flattened, its theoretical width increases and, thus, the volume of voids is likely to decrease, leading to higher density values, as reported by Lambiase et al. [57]. A reduction in void density has also been reported when temperature increases [55]. Although many interactions are significant, the most important one corresponds to extrusion multiplier·printing temperature (Figure 8b). If a low temperature of 200 °C is selected, high porosity will be obtained regardless of the extrusion multiplier value. On the contrary, if a high temperature of 220 °C is chosen, lower porosity will be achieved with a high extrusion multiplier value of 1. This suggests that, at low temperatures, material flow could slow down due to insufficient melting of the material [48], regardless of the extrusion multiplier that is used. On the contrary, at high temperatures, and for a fixed layer height value, the higher the extrusion multiplier, the wider the bead width, because its cross-sectional area increases, and a lower porosity will be achieved as expected [46,47]. It should also be considered that, since the printing direction alternates in consecutive layers, the distance between the material and the nozzle outlet will

change frequently. This could also affect porosity when comparing the rectilinear pattern with other patterns in which distance is almost constant during the printing operation, for example, the grid pattern.

Table 3 contains the main characteristics of the linear regression models.

Table 3. R^2 (adj) (%) and main effects of the regression models for Edx, Edy, Edz, Edt and P.

Response	R^2 (adj) (%)	Variable	Effect
Edx	99.39	LH	3.01
		TE	0.81
		PS	0.74
		LH·TE	0.54
Edy	97.69	LH	3.09
		TE	0.91
		LH·TE	0.64
		PS	0.56
Edz	69.10	PS	0.66
		LH·PS	0.58
Edt	96.86	LH	2.31
		TE	0.57
		LH·PS	0.33
P	93.38	LH	11.53
		PS	4.09
		LH·PS	0.52
		AC·EM	0.73

The terms that most influence dimensional error in the X and Y directions are layer height (with an important effect) and temperature, while, in the Z direction, the most influential terms are print speed and the interaction between layer height and print speed (with similar effects). Porosity depends mainly on layer height and print speed. A high fit of above 90% was obtained in all cases, except for Edz, with a fit around 69%.

3.3. Multi-Objective Optimization

Dimensional error along the X and Y directions and porosity depend mainly on layer height and temperature, but dimensional error along the Z direction is related to print speed. This corresponds to opposite objectives. For this reason, multi-objective optimization was carried out using the Derringer—Suich desirability function, in order to determine the printing conditions that simultaneously minimize dimensional error and provide a target porosity value.

The results of the first optimization study (minimization of Edt and target value of 20% for porosity) are presented in Table 4.

Table 4. Results of the first multi-objective optimization study.

Importance	LH (mm)	PS (mm/s)	ME	PT (°C)	Composite Desirability
Equal	0.1	40	0.94	200	0.942
Higher for Edt	0.1	40	0.94	200	0.941
Higher for P	0.1	40	0.94	200	0.943

In all cases, i.e., when both responses are given the same importance or when each of the responses has greater importance, a low layer height of 0.1 mm, a high print speed of 40 mm/s, a low extrusion multiplier of 0.94 and a low temperature are recommended. In all cases, composite desirability values are higher than 0.94.

The results of the second optimization study (minimization of Edz and target value of 20% for porosity) are presented in Table 5.

Table 5. Results of the second multi-objective optimization study.

Importance	LH (mm)	PS (mm/s)	ME	PT (°C)	Composite Desirability
Equal	0.3	40	1	220	0.959
Higher for Edz	0.3	40	1	220	0.943
Higher for P	0.3	40	1	220	0.974

The same results were obtained when both responses are given the same importance value or when one of the responses has higher importance. In all cases, a high layer height of 0.3 mm, a high print speed of 40 mm/s, a high extrusion multiplier of 1 and a high temperature of 220 °C are recommended. This reveals the great influence of Edz in the optimization process: if Edz is to be minimized instead of Edt, the values of all the parameters except that of print speed should be changed. An especially high desirability value of above 0.97 was obtained when more importance is given to porosity.

As for the use of other commercially available PLA-containing filaments, either with bronze [58] (with a filament density of 3.9 g/cm^3) or with stainless-steel particles (with a filament density of 3.13 g/cm^3) [59], they would behave similarly to the copper-filled material in terms of dimensional accuracy and roughness according to our preliminary tests. When comparing composites with different metallic fillers, it has been shown that the addition of both copper and iron increases the flow behavior of the composites compared to their respective original matrices [60,61]. On the other hand, Nikzad et al. [13] compared the storage modulus of two composites containing either Cu or Fe with the same particle size of 45 μm. In both cases, the storage modulus increased up to a certain percentage of filler, and then decreased at higher loadings.

4. Conclusions

In the present work, results on dimensional accuracy and porosity of FFF 3D-printed copper-filled PLA parts are presented. The main conclusions of the research are as follows:

- Relative dimensional errors of up to 5.8% in the X and Y directions were found. They depend mainly on the layer height and the printing temperature.
- Lower relative dimensional errors of up to 3.5% were determined in the Z direction. They are mainly influenced by the print speed and the interaction between print speed and layer height.
- Porosity values ranged from 7.46% to 35.60%, depending on the 3D printing conditions selected, while the target value was 20%. This is mainly related to the layer height and temperature.
- When the total relative error is minimized and a target porosity value of 20% is defined, the best solution corresponds to a low layer height of 0.1 mm, a high print speed of 40 mm/s, a low extrusion multiplier of 0.94 and a low temperature of 200 °C. On the other hand, if only the relative error along the Z axis, and porosity, are considered, a high layer height of 0.3 mm, a high extrusion multiplier of 1 and a high temperature of 220 °C are recommended.

The study will help to define suitable 3D-printing conditions, i.e., -layer height, print speed, and printing temperature-, when metal-filled filaments are used in FFF processes.

Author Contributions: Conceptualization, I.B.-C.; methodology, I.B.-C. and M.S.-A.; software, M.S.-A.; validation, I.B.-C. and M.S.-A.; formal analysis, I.B.-C.; investigation I.B.-C. and M.S.-A.; resources, I.B.-C.; data curation, I.B.-C. and M.S.-A.; writing—original draft preparation, M.S.-A.; writing—review and editing, I.B.-C.; visualization, I.B.-C. and M.S.-A.; supervision, I.B.-C.; project administration, I.B.-C.; funding acquisition, I.B.-C. All authors have read and agreed to the published version of the manuscript.

Funding: The present research was co-financed by the European Union Regional Development Fund within the framework of the ERDF Operational Program of Catalonia 2014–2020 with a grant of 50% of total cost eligible, project BASE3D, grant number 001-P-001646.

Data Availability Statement: Data are available upon request.

Acknowledgments: The authors would like to thank Ramón Casado and Javier Rodelas for their help with the experimental tests.

Conflicts of Interest: The authors declare no conflict of interest.

References

1. Liu, B.; Wang, Y.; Lin, Z.; Zhang, T. Creating metal parts by Fused Deposition Modeling and Sintering. *Mater. Lett.* **2020**, *263*, 127252. [CrossRef]
2. Ramazani, H.; Kami, A. Metal FDM, a new extrusion-based additive manufacturing technology for manufacturing of metallic parts: A review. *Prog. Addit. Manuf.* **2022**, *7*, 609–626. [CrossRef]
3. Konieczny, J.; Rdzawski, Z. Antibacterial properties of copper and its alloys. *Arch. Mater. Sci. Eng.* **2012**, *56*, 53–60.
4. Fattah-Alhosseini, A.; Imantalab, O. Effect of accumulative roll bonding process on the electrochemical behavior of pure copper. *J. Alloys Compd.* **2015**, *632*, 48–52. [CrossRef]
5. Alfantazi, A.M.; Ahmed, T.M.; Tromans, D. Corrosion behavior of copper alloys in chloride media. *Mater. Des.* **2009**, *30*, 2425–2430. [CrossRef]
6. Lewis, A.; Keevil, C. *Antibacterial Properties of Alloys and Its Alloys in HVAC\&R Systems*; International Copper Association: New York, NY, USA, 2004.
7. Vidakis, N.; Petousis, M.; Michailidis, N.; Grammatikos, S.; David, C.N.; Mountakis, N.; Argyros, A.; Boura, O. Development and Optimization of Medical-Grade MultiFunctional Polyamide 12-Cuprous Oxide Nanocomposites with Superior Mechanical and Antibacterial Properties for Cost-Effective 3D Printing. *Nanomaterials* **2022**, *12*, 534. [CrossRef]
8. Buj-Corral, I.; Sanz-Fraile, H.; Ulldemolins, A.; Tejo-Otero, A.; Domínguez-Fernández, A.; Almendros, I.; Otero, J. Characterization of 3D Printed Metal-PLA Composite Scaffolds for Biomedical Applications. *Polymers* **2022**, *14*, 2754. [CrossRef]
9. Alam, F.; Shukla, V.R.; Varadarajan, K.M.; Kumar, S. Microarchitected 3D printed polylactic acid (PLA) nanocomposite scaffolds for biomedical applications. *J. Mech. Behav. Biomed. Mater.* **2020**, *103*, 103576. [CrossRef]
10. León-Patiño, C.A.; Rodriguez-Ortiz, G.; Aguilar-Reyes, E.A. Fabrication and thermal properties of copper-based composites. In Proceedings of the Materials Science and Technology Conference and Exhibition 2009, MS and T'09, Pittsburgh, PA, USA, 25–29 October 2009; Volume 3, pp. 1848–1855.
11. Timbs, K.; Khatamifar, M.; Antunes, E.; Lin, W. Experimental study on the heat dissipation performance of straight and oblique fin heat sinks made of thermal conductive composite polymers. *Therm. Sci. Eng. Prog.* **2021**, *22*, 100848. [CrossRef]
12. Hwang, S.; Reyes, E.I.; Moon, K.-s.; Rumpf, R.C.; Kim, N.S. Thermo-mechanical Characterization of Metal/Polymer Composite Filaments and Printing Parameter Study for Fused Deposition Modeling in the 3D Printing Process. *J. Electron. Mater.* **2015**, *44*, 771–777. [CrossRef]
13. Nikzad, M.; Masood, S.H.; Sbarski, I. Thermo-mechanical properties of a highly filled polymeric composites for Fused Deposition Modeling. *Mater. Des.* **2011**, *32*, 3448–3456. [CrossRef]
14. Vidakis, N.; Petousis, M.; Papadakis, V.M.; Mountakis, N. Multifunctional Medical Grade Resin with Enhanced Mechanical and Antibacterial Properties: The Effect of Copper Nano-Inclusions in Vat Polymerization (VPP) Additive Manufacturing. *J. Funct. Biomater.* **2022**, *13*, 258. [CrossRef]
15. Rane, K.; Strano, M. A comprehensive review of extrusion-based additive manufacturing processes for rapid production of metallic and ceramic parts. *Adv. Manuf.* **2019**, *7*, 155–173. [CrossRef]
16. Wu, G.; Langrana, N.A.; Sadanji, R.; Danforth, S. Solid freeform fabrication of metal components using fused deposition of metals. *Mater. Des.* **2002**, *23*, 97–105. [CrossRef]
17. Singh, B.; Kumar, R.; Chohan, J.S.; Singh, S.; Pruncu, C.I.; Scutaru, M.L.; Muntean, R. Investigations on melt flow rate and tensile behaviour of single, double and triple-sized copper reinforced thermoplastic composites. *Materials* **2021**, *14*, 3504. [CrossRef]
18. Phani Babu, V.V.; GB, V.K. A review on 3D printing process on metals and their surface roughness and dimensional accuracy. *Mater. Today Proc.* **2022**, *64*, 523–530. [CrossRef]
19. Fafenrot, S.; Grimmelsmann, N.; Wortmann, M.; Ehrmann, A. Three-dimensional (3D) printing of polymer-metal hybrid materials by fused deposition modeling. *Materials* **2017**, *10*, 1199. [CrossRef]
20. Kottasamy, A.; Samykano, M.; Kadirgama, K.; Rahman, M.; Noor, M.M. Experimental investigation and prediction model for mechanical properties of copper-reinforced polylactic acid composites (Cu-PLA) using FDM-based 3D printing technique. *Int. J. Adv. Manuf. Technol.* **2022**, *119*, 5211–5232. [CrossRef]
21. Balamurugan, K.; Venkata Pavan, M.; Ahamad Ali, S.K.; Kalusuraman, G. Compression and flexural study on PLA-Cu composite filament using FDM. *Mater. Today Proc.* **2021**, *44*, 1687–1691. [CrossRef]
22. Prajapati, A.R.; Rajpurohit, S.R.; Patadiya, N.H.; Dave, H.K. Analysis of Compressive Strength of 3D Printed PLA Part. In *Lecture Notes in Mechanical Engineering*; Springer: Singapore, 2021; pp. 295–304. ISBN 9789811591167.
23. Sa'ude, N.; Masood, S.H.; Nikzad, M.; Ibrahim, M. Dynamic Mechanical Properties of Copper-ABS Composites for FDM Feedstock. *Int. J. Eng. Res. Appl.* **2013**, *3*, 1257–1263.
24. Sa'ude, N.; Ibrahim, M.; Ibrahim, M.H.I.; Wahab, M.S.; Haq, R.; Marwah, O.M.F.; Khirotdin, R.K. Additive manufacturing of copper-ABS filament by fused deposition modeling (FDM). *J. Mech. Eng.* **2018**, *5*, 23–32.

25. Petousis, M.; Vidakis, N.; Mountakis, N.; Papadakis, V.; Kanellopoulou, S.; Gaganatsiou, A.; Stefanoudakis, N.; Kechagias, J. Multifunctional Material Extrusion 3D-Printed Antibacterial Polylactic Acid (PLA) with Binary Inclusions: The Effect of Cuprous Oxide and Cellulose Nanofibers. *Fibers* **2022**, *10*, 52. [CrossRef]
26. Buj-Corral, I.; Sivatte-Adroer, M. Multi-Objective Optimization of Material Removal Rate and Tool Wear in Rough Honing Processes. *Machines* **2022**, *10*, 83. [CrossRef]
27. Islam, M.N.; Boswell, B.; Pramanik, A. An investigation of dimensional accuracy of parts produced by three-dimensional printing. In Proceedings of the World Congress on Engineering, London, UK, 3–5 July 2013; 1 WCE 2013.
28. Vidakis, N.; David, C.; Petousis, M.; Sagris, D.; Mountakis, N.; Moutsopoulou, A. The effect of six key process control parameters on the surface roughness, dimensional accuracy, and porosity in material extrusion 3D printing of polylactic acid: Prediction models and optimization supported by robust design analysis. *Adv. Ind. Manuf. Eng.* **2022**, *5*, 100104. [CrossRef]
29. Vidakis, N.; David, C.; Petousis, M.; Sagris, D.; Mountakis, N. Optimization of key quality indicators in material extrusion 3D printing of acrylonitrile butadiene styrene: The impact of critical process control parameters on the surface roughness, dimensional accuracy, and porosity. *Mater. Today Commun.* **2023**, *34*, 105171. [CrossRef]
30. Luis-Pérez, C.J.; Buj-Corral, I.; Sánchez-Casas, X. Modeling of the influence of input am parameters on dimensional error and form errors in pla parts printed with fff technology. *Polymers* **2021**, *13*, 4152. [CrossRef] [PubMed]
31. Rahman, H.; John, T.D.; Sivadasan, M.; Singh, N.K. Investigation on the Scale Factor applicable to ABS based FDM Additive Manufacturing. *Mater. Today Proc.* **2018**, *5*, 1640–1648. [CrossRef]
32. Ceretti, E.; Ginestra, P.; Neto, P.I.; Fiorentino, A.; Da Silva, J.V.L. Multi-layered Scaffolds Production via Fused Deposition Modeling (FDM) Using an Open Source 3D Printer: Process Parameters Optimization for Dimensional Accuracy and Design Reproducibility. *Procedia CIRP* **2017**, *65*, 13–18. [CrossRef]
33. Nancharaiah, T.; Raju, D.R.; Raju, V.R. An experimental investigation on surface quality and dimensional accuracy of FDM components. *Int. J. Emerg. Technol.* **2010**, *1*, 106–111.
34. Pennington, R.C.; Hoekstra, N.L.; Newcomer, J.L. Significant factors in the dimensional accuracy of fused deposition modelling. *Proc. Inst. Mech. Eng. Part E J. Process Mech. Eng.* **2005**, *219*, 89–92. [CrossRef]
35. Caminero, M.Á.; Chacón, J.M.; García-Plaza, E.; Núñez, P.J.; Reverte, J.M.; Becar, J.P. Additive manufacturing of PLA-based composites using fused filament fabrication: Effect of graphene nanoplatelet reinforcement on mechanical properties, dimensional accuracy and texture. *Polymers* **2019**, *11*, 799. [CrossRef] [PubMed]
36. Karageorgiou, V.; Kaplan, D. Porosity of 3D biomaterial scaffolds and osteogenesis. *Biomaterials* **2005**, *26*, 5474–5491. [CrossRef] [PubMed]
37. Egan, P.F.; Shea, K.A.; Ferguson, S.J. Simulated tissue growth for 3D printed scaffolds. *Biomech. Model. Mechanobiol.* **2018**, *17*, 1481–1495. [CrossRef] [PubMed]
38. Too, M.H.; Leong, K.F.; Chua, C.K.; Du, Z.H.; Yang, S.F.; Cheah, C.M.; Ho, S.L. Investigation of 3D non-random porous structures by fused deposition modelling. *Int. J. Adv. Manuf. Technol.* **2002**, *19*, 217–223. [CrossRef]
39. Buj-Corral, I.; Bagheri, A.; Domínguez-Fernández, A.; Casado-López, R. Influence of infill and nozzle diameter on porosity of FDM printed parts with rectilinear grid pattern. *Procedia Manuf.* **2019**, *41*, 288–295. [CrossRef]
40. Ben Ali, N.; Khlif, M.; Hammami, D.; Bradai, C. Mechanical and morphological characterization of spherical cell porous structures manufactured using FDM process. *Eng. Fract. Mech.* **2019**, *216*, 106527. [CrossRef]
41. Karimi, M.; Asadi-Eydivand, M.; Abolfathi, N.; Chehrehsaz, Y.; Solati-Hashjin, M. The effect of pore size and layout on mechanical and biological properties of 3D-printed bone scaffolds with gradient porosity. *Polym. Compos.* **2023**, *44*, 1343–1359. [CrossRef]
42. Buj-Corral, I.; Bagheri, A.; Sivatte-Adroer, M. Effect of Printing Parameters on Dimensional Error, Surface Roughness and Porosity of FFF Printed Parts with Grid Structure. *Polymers* **2021**, *13*, 1213. [CrossRef]
43. Colorfabb Technical Datasheet of Copperfill. Available online: https://colorfabb.com/media/datasheets/tds/colorfabb/TDS_E_ColorFabb_CopperFill.pdf (accessed on 20 August 2023).
44. Derringer, G.; Suich, R. Simultaneous Optimization of Several Response Variables. *J. Qual. Technol.* **2018**, *12*, 214–219. [CrossRef]
45. Frunzaverde, D.; Cojocaru, V.; Bacescu, N.; Ciubotariu, C.R.; Miclosina, C.O.; Turiac, R.R.; Marginean, G. The Influence of the Layer Height and the Filament Color on the Dimensional Accuracy and the Tensile Strength of FDM-Printed PLA Specimens. *Polymers* **2023**, *15*, 2377. [CrossRef]
46. Zharylkassyn, B.; Perveen, A.; Talamona, D. Effect of process parameters and materials on the dimensional accuracy of FDM parts. *Mater. Today Proc.* **2021**, *44*, 1307–1311. [CrossRef]
47. Butt, J.; Bhaskar, R.; Mohaghegh, V. Analysing the effects of layer heights and line widths on FFF-printed thermoplastics. *Int. J. Adv. Manuf. Technol.* **2022**, *121*, 7383–7411. [CrossRef]
48. Kumar, N.; Jain, P.K.; Tandon, P.; Pandey, P.M. Investigation on the effects of process parameters in CNC assisted pellet based fused layer modeling process. *J. Manuf. Process.* **2018**, *35*, 428–436. [CrossRef]
49. Ćwikła, G.; Grabowik, C.; Kalinowski, K.; Paprocka, I.; Ociepka, P. The influence of printing parameters on selected mechanical properties of FDM/FFF 3D-printed parts. *IOP Conf. Ser. Mater. Sci. Eng.* **2017**, *227*, 012033. [CrossRef]
50. Geng, P.; Zhao, J.; Wu, W.; Ye, W.; Wang, Y.; Wang, S.; Zhang, S. Effects of extrusion speed and printing speed on the 3D printing stability of extruded PEEK filament. *J. Manuf. Process.* **2019**, *37*, 266–273. [CrossRef]

51. Stojković, J.R.; Turudija, R.; Vitković, N.; Sanfilippo, F.; Păcurar, A.; Pleşa, A.; Ianoşi-Andreeva-Dimitrova, A.; Păcurar, R. An Experimental Study on the Impact of Layer Height and Annealing Parameters on the Tensile Strength and Dimensional Accuracy of FDM 3D Printed Parts. *Materials* **2023**, *16*, 4574. [CrossRef]
52. Brackett, J.; Cauthen, D.; Condon, J.; Smith, T.; Gallego, N.; Kunc, V.; Duty, C. The impact of infill percentage and layer height in small-scale material extrusion on porosity and tensile properties. *Addit. Manuf.* **2022**, *58*, 103063. [CrossRef]
53. Dave, H.K.; Rajpurohit, S.R.; Patadiya, N.H.; Dave, S.J.; Sharma, K.S.; Thambad, S.S.; Srinivasn, V.P.; Sheth, K. V Compressive strength of PLA based scaffolds: Effect of layer height, infill density and print speed. *Int. J. Mod. Manuf. Technol.* **2019**, *11*, 21–27.
54. Buj-Corral, I.; Petit-Rojo, O.; Bagheri, A.; Minguella-Canela, J. Modelling of porosity of 3D printed ceramic prostheses with grid structure. *Procedia Manuf.* **2017**, *13*, 770–777. [CrossRef]
55. Garzon-Hernandez, S.; Arias, A.; Garcia-Gonzalez, D. A continuum constitutive model for FDM 3D printed thermoplastics. *Compos. Part B Eng.* **2020**, *201*, 108373. [CrossRef]
56. Darsin, M.; Mahardika, N.A.; Jatisukamto, G.; Ramadhan, M.E.; Fachri, B.A.; Hussin, M.S. Effect of 3D Printing Parameters on Dimensional Accuracy Using eSteel Filaments. *J. 3D Print. Addit. Manuf.* **2022**, 1–7. [CrossRef]
57. Lambiase, F.; Scipioni, S.I.; Paoletti, A. Mechanical characterization of FDM parts through instrumented flat indentation. *Int. J. Adv. Manuf. Technol.* **2023**, *125*, 4201–4211. [CrossRef]
58. Colorfabb Technical Datasheet of Bronzefill. Available online: https://colorfabb.com/media/datasheets/tds/colorfabb/TDS_E_ColorFabb_BronzeFill.pdf (accessed on 20 August 2023).
59. Colorfabb Technical Datasheet of Steelfill. Available online: https://colorfabb.com/media/datasheets/tds/colorfabb/TDS_E_ColorFabb_SteelFill.pdf (accessed on 20 August 2023).
60. Isa, N.M.A.; Sa'ude, N.; Ibrahim, M.; Hamid, S.M.; Kamarudin, K. A Study on Melt Flow Index on Copper-ABS for Fused Deposition Modeling (FDM) Feedstock. *Appl. Mech. Mater.* **2015**, *773–774*, 8–12. [CrossRef]
61. Garg, H.; Singh, R. Investigations for melt flow index of Nylon6-Fe composite based hybrid FDM filament. *Rapid Prototyp. J.* **2016**, *22*, 338–343. [CrossRef]